Available online at www.sciencedirect.com
ScienceDirect
Proceedings of the Combustion Institute 33 (2011) 3447–3454
Proceedings of the Combustion Institute
www.elsevier.com/locate/proci

Concept and combustion characteristics of the high-luminescence flame for thermophotovoltaic systems

Yueh-Heng Li [a,*], Chih-Yung Wu [b], Hong-Yuan Li [a], Yei-Chin Chao [a,**]

[a] Institute of Aeronautics and Astronautics, National Cheng Kung University, Tainan 701, Taiwan, ROC
[b] Department of Electro-Optical Science and Engineering, Kao Yuan University, Kaohsiung County, 1821, Taiwan, ROC

Available online 9 September 2010

Abstract

The thermophotovoltaic (TPV) power system mainly consists of a heat source, an emitter and a photovoltaic (PV) cell array. One of the major deficiencies leading to the relatively low overall efficiency of the TPV power system is the spectral mismatch between the emitter radiation and the quantum efficiency peak of the PV cells. Therefore, application of high-luminescent-flame in the visible range is a cost-effective method to enhance the radiant efficiency of a small TPV system. The concept of the high-luminescent-flame combustor is proposed with central-porous liquid fuel-film injection of *n*-heptane and trace amount of iron pentacarbonyl, and an emitter tube. The metal-porous fuel-film injection is an effective method to increase contact surface and thermal conduction for liquid fuel vaporization and for flame stabilization. Chemiluminescence measurement and Abel deconvolution are further performed to identify the flame structure in two different porous materials, bronze and stainless steel, respectively. Flame structure and stabilization mechanism in the chamber can be related to the tribrachial flame. The radiant intensity of the iron pentacarbonyl flame is significantly enhanced by fivefold, and flame color turns to sliver-white. Inserting an emitter tube in the combustor can further effectively integrate the radiation from the flame luminosity and emitter incandescence, and improve the radiant efficiency of the TPV system.
© 2010 The Combustion Institute. Published by Elsevier Inc. All rights reserved.

Keywords: Meso-scale combustor; Fuel-film; Porous medium; Thermophotovoltaic (TPV); Iron pentacarbonyl

1. Introduction

Meso-scale combustion has been considered as one of the potential solutions for the increasing demand of higher-density power supplies for the miniaturized devices [1,2]. Simultaneous production of electric power and heat can be achieved by means of a thermophotovoltaic (TPV) power generator in fuel-fired residential and commercial heating appliances. Therefore, research interest in TPV cogeneration and combustion-driven TPV systems [3–5] has received intensive attention. In general, the TPV power system mainly consists of a heat source, an emitter and a photovoltaic (PV) cell array. The overall efficiency of a combustion-driven TPV power system is ultimately relevant to the radiant efficiency of an emitter and the quantum efficiency of PV cells. As regards

* Corresponding author. Fax: +886 6 238 9940.
** Corresponding author. Fax: +886 6 238 9940.
E-mail addresses: yuehheng.li@gmail.com (Y.-H. Li), ycchao@mail.ncku.edu.tw (Y.-C. Chao).

1540-7489/$ - see front matter © 2010 The Combustion Institute. Published by Elsevier Inc. All rights reserved.
doi:10.1016/j.proci.2010.06.142

the PV cells, there are two main approaches of realizing the TPV conversion process. One uses silicon solar cells (1.1 eV). The other involves using low band-gap TPV cells such as GaSb cells (0.72 eV) [6] and InGaAsSb cells (0.53 eV) [7]. Lowering the band-gap of PV cells will allow more effective photons with lower energy to be absorbed by the PV cells and creates electron–hole pairs. Nevertheless, a low band-gap photovoltaic cell has good quantum efficiencies in the visible-to-near-infrared range, in contrast to the infrared radiation of the conventional TPV emitters. This spectral mismatch leads to principle energy loss on the overall efficiency of nowadays TPV power systems. Therefore, advanced TPV researches emphasize on improvement and development of low band-gap photovoltaic cells [6,7], selective emitters [8,9], and spectral control devices [10] to filter the radiant and to reflect the non-photon-convertible radiation back to the radiator. Nonetheless, expense and complex manufacture of these components are essential concerns, so that it is still not extensively used.

In this paper, the concept of integrating the enhanced visible radiation from the hydrocarbon flame and the near-infrared radiation from the emitter is proposed to ameliorate the spectral mismatch in the TPV system. Therefore, the objective of this paper is to design a novel mesoscale high-luminescent-flame combustor which releases broadband radiation for PV cells, and to examine its combustion and flame stabilization characteristics.

2. Concept of the high-luminescence flame

The spectral mismatch between the emitter radiation and the PV cells can be resolved by enhancing the flame radiation in the visible range, i.e., the high-luminescence flame. It has been shown in the study of CO/CH_4 blended fuel that flame luminosity increases with concentration ratio of CO in the CO/CH_4 mixture [11]. The spectral analysis result appears that the broadband spectrum in the visible range from 300 to 700 nm is significantly enhanced as the CO concentration ratio goes higher than 50%. This high flame luminosity of CO/CH_4 flame is shown to be due to decomposition of trace amount of metal carbonyls [12] in forms of iron pentacarbonyl ($Fe[CO]_5$) and to a lesser extent of nickel tetracarbonyl ($Ni[CO]_4$), which comes from reactions of CO with the iron content in the storage cylinder and piping. Besides, the unintended addition of trace amount of iron pentacarbonyl to CO flames may affect flame speed, ignition and extinction [13,14].

Iron pentacarbonyl is flammable and soluble in organic solvents, such as *n*-heptane. It is advantageous to perform high-luminescence flames by means of adding iron pentacarbonyl in liquid hydrocarbon fuels. For application of liquid fuels in small TPV systems, the concept of liquid fuel-film proposed by Sirignano et al. [15,16] is more appropriate than spray in consideration of small combustor size relative to spray volume, fuel evaporation, and flame stabilization. However, the conventional wall fuel-film combustor design falls against the fundamental requirements of an emitter in the small TPV system. Consequently, a new mesoscale fuel-film combustor for high-luminescent-flame TPV system is necessitated.

3. Concept and combustion characteristics of the central-porous fuel-film combustor

3.1. Concept and apparatus

Figure 1 illustrates the configuration of the miniature central-porous liquid-film combustor with an emitter tube. The liquid fuel is injected smoothly from two inlet ports into the fuel trough using a syringe pump, which provides continuous fuel inlet in c.c.-per-hour scale. The liquid fuel may penetrate through the porous cap and form a liquid-film on the surface. The air, metered by an electronic flowmeter, is injected tangentially above the fuel ports with a swirl number around 0.6 [17]. Swirling air entering the cylindrical chamber serves to enhance fuel–air mixing, increase residence time, and provide a recirculation mechanism to stabilize the flame. The metal-porous medium provides large surface area as well as heat recuperation from flame for fuel-film vaporization. Moreover, in order to simultaneously attain flame luminosity from the iron pentacarbonyl-doped hydrocarbon flames and thermal radiance from the emitter, an emitter tube is used in the combustor.

The combustion chamber consists of four parts: the main combustion chamber of 14 mm inside diameter (ID) and 60 mm in length with swirling air inlet ports, a chamber set with a fuel trough of 6 mm ID and fuel inlet ports, a porous

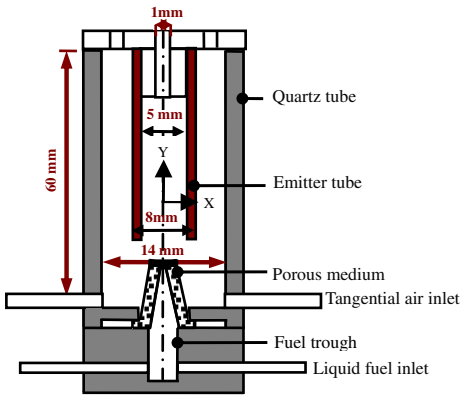

Fig. 1. Schematic diagram of the proposed combustor.

medium and an emitter tube [18]. The combustion chamber is made of quartz, and allows both flame luminosity and emitter radiation to PV cells. The emitter tube, made of silicon carbide, is used as a broadband emitter for TPV and operates in the temperature range 1000–1600 K. Flames are expected to burn along the emitter tube, and then to heat up the emitter from outside and inside. This approach can effectively superpose the flame luminosity and emitter radiation together. The porous mediums, two of them made of uniformed stainless steel and bronze powders of 20 μm, are conical in shape with a dimension of 4 mm in diameter on top and 6.5 mm in the bottom and 10 mm in length.

Air is supplied by an air compressor, then dried and metered with a mass flowmeter calibrated in the range of 0–60 standard l/min. The surface temperature of the porous medium is measured by a non-invasively IR thermometer. The uncertainty of the temperature measurement is estimated to be 10 K. Concentrations of exhaust NO_x and CO are measured with an infrared gas analyzers (MRU VarioPlus) calibrated in the range of 0–600 ppm with an uncertainty of ±2 and ±5 ppm, referring to 12% O_2, respectively. The radiation spectra from flames and the emitter are measured by the fluorescence spectrometer (USB4000-FL, Ocean Optics) covering the 360–1000 nm wavelength range. The flame chemiluminescence images for flame structural characteristics are taken with their respective narrow bandpass filters through a 14-bit intensified CCD camera at 307 nm for OH*, 430 nm for CH* and 515 nm for C_2^*. Since the chamber is cylindrical in geometry, appropriate analysis of the flame images requires deconvolution of the line-integrated image. The inverse Abel transform [19] is adopted for all chemiluminescence images.

3.2. Flame structure and combustion characteristics

The thermal conductivity and specific heat of the central-porous medium significantly influence the thermal recuperating mechanism and flame stabilization in a meso-scale combustor. Figure 2 shows the effect of different porous materials of stainless steel and bronze of identical pore size (~20 μm) on flame anchoring position. The flame structure with the bronze porous medium combustor indicates two layers of flame; one is the inner flame acting like a pilot flame, and the other is the outer flame behaving as a swirl flame. The flame base locates in the vicinity of the porous cap top. No significant change in flame anchoring and flame structure can be found in Fig. 2 as the air flow rate is increased. For the stainless steel porous medium, the flame structure looks like a swirl flame and the flame base anchors on the lateral surface of the porous cap. When the air flow rate increases, the flame anchoring position moves

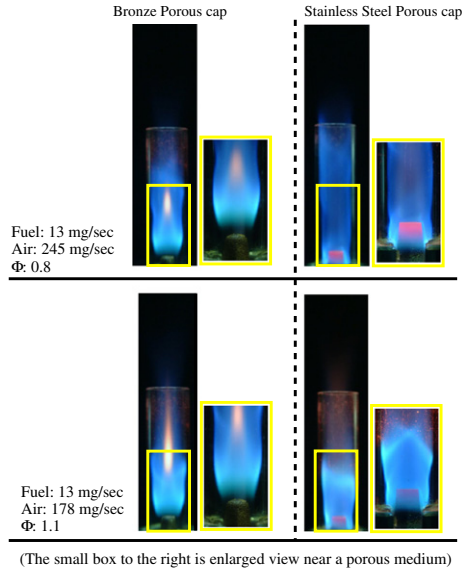

Fig. 2. Flame mode and anchor position for different porous materials.

upstream, and then the red hot spot on the porous cap also becomes larger and brighter. Apparently, there are different flame stabilization mechanisms for the two different porous material cases.

In general, stainless steel has a lower thermal conductivity (16.2 W/m K) so that its temperature takes longer to reach a new equilibrium condition. Moreover, stainless steel also has smaller thermal diffusivity ($\sim 4.05 \times 10^{-6}$ m^2/s) and is better to store heat from flames. The important point is that the stainless steel reduces overall heat loss to the system enabling higher surface temperature. A hot spot on the porous cap offers a flame stabilization mechanism because it locally accelerates liquid fuel vaporization. The produced fuel vapor then mixes with fresh swirling air near the porous cap, leading to rapid reaction along the lateral surface of the cap. Similar to flame spread along a flat plate, it is noted that the flame stabilization mechanism in the stainless steel porous combustor is related to the tribrachial flame structure. Figure 3 presents the deconvoluted chemiluminescence images of OH*, CH*, C_2^* and the corresponding flame image near the stainless steel porous cap at an airflow rate of 1.7 m/s and a heptanes flow rate of 10.93 mg/s, for a resulting equivalence ratio (Φ) of 1.07. Figure 3(b) displays that C_2^* radicals are distributed in the two flame layers and their concentration peaks in the layer near the wall. The C_2^* radical concentration indicates highly rich zones in these regions. In contrast, the OH* concentration is high near the wall and it fades away toward the porous medium (Fig 3c), revealing the main reaction zone near the wall. Moreover, CH* radicals are extensively congregated in the regions near the wall

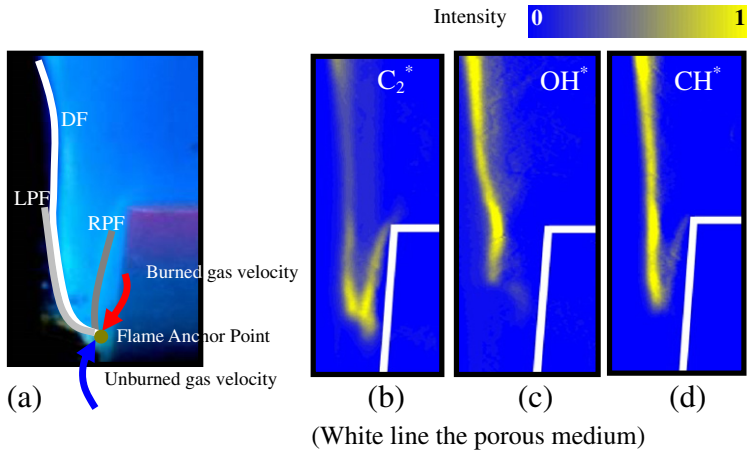

Fig. 3. (a) Proposed tribrachial flame structure and flame image near the stainless steel porous media, and chemiluminescence images of excited (b) C_2^*, (c) OH*, and (d) CH*.

and near the porous medium (Fig. 3d). The two concentration branches overlap at the point close to the flame base near the porous surface. These images confirm that the flame structure is composed of two-layer flames in the chamber consisting of a lean and a rich premixed flame wings together with a trailing diffusion flame. All of these flames extend from a single point at the flame base, which corresponds to the stabilization point of the tribrachial flame which anchors the flame. A diffusion flame (DF) burns between the wall and the porous cap. A rich premixed flame (RFP) exists close to porous cap and forms a boundary-layer-like flame sheet along it. The lean premixed flame (LPF) of the tribrachial structure tangling with the diffusion flame is difficult to see due to its low luminosity, but it can vaguely be identified near the wall. The flame anchoring point occurs where there is a balance between the propagation of apex point of the tribrachial flame and the supply of fuel/air mixture which then balances the supply and consumption of flammable (or stoichiometric) fuel–air mixture, as shown in Fig 3a.

On the other hand, in the bronze porous case, the flame is stationary on top of the porous cap in the same condition with the case in Fig. 3. The bluff body nature of the porous cap generates a wake recirculation behind it. The recirculation zone provides a relative low velocity field for flame to anchors in this region, as shown in Fig 4a. The OH*, CH* and C_2^* radicals distribute in two flame layers as shown in Fig. 4b–d. The flame structure looks similar to that of the stainless steel case, except that the flame anchors above the porous cap. A diffusion flame layer, depicted by peak CH* and C_2^* radical concentrations and main OH* distribution, can easily be identified. . A diffusion flame (DF) and a lean premixed flame (LPF) tangle and burn along the chamber wall, while a rich premixed flame (RPF) inclines to the combustor axis. The flame anchoring position is quite stable due to the high thermal conductivity of the bronze. Hence, despite different flame anchoring phenomena, the flame stabilization mechanism in combustors of two different porous materials is mainly a typical tribrachial flame [20,21].

Periodic flame pulsation may happen in bronze porous cap combustor, as shown in Fig. 5a. Flame anchoring position will suddenly move upstream and engulf the whole porous cap, and then recess and go back to the original position. Undoubtedly, the surface temperature on the porous medium influences the flame stability substantially. Figure 5b–d shows the measured time-trace surface temperatures near the top-head of the two material porous caps in different operating condition by a non-invasively IR thermometer. It is observed that the surface temperature of the bronze cap shows high-frequency fluctuations for equivalence ratio 0.8, but it becomes more stable for the stainless steel case, as shown in Fig. 5b. Generally, bronze has a higher thermal conductivity ($\sim$385 W/m K) and its thermal diffusivity ($\sim 1.12 \times 10^{-4}$ m^2/s) is almost two orders of magnitude higher than that of stainless steel. Hence, the heat from the flame would effectively conduct away from the surface and be absorbed by the liquid fuel. The unbalance between the fuel flow rate and fuel evaporating rate triggers the surface temperature fluctuation of the bronze porous cap. This fluctuation caused by the over-heated porous cap induces flame instability and oscillations in the combustor. Bronze porous cap absorbs heat from the flame, and the heated metal-porous cap enhances vaporization of the liquid fuel until dry-out of the fuel-film. The excess gaseous heptane will reduce the permeability of the porous medium and temporarily retard liquid fuel supply. The cold liquid fuel will rush in and flush the hot

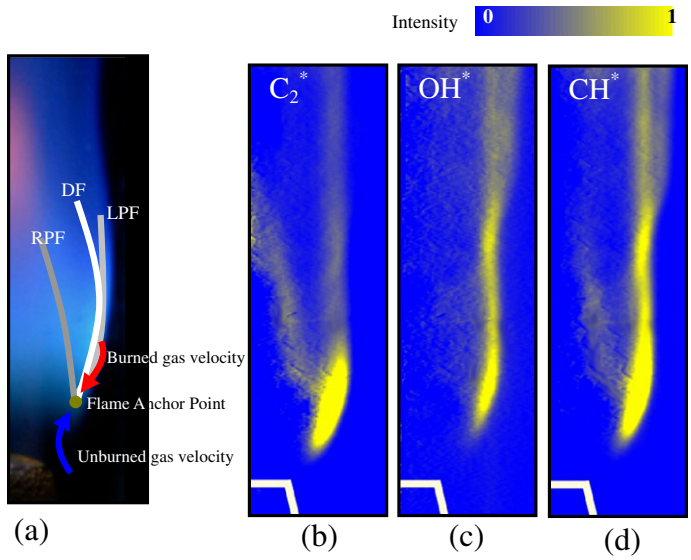

Fig. 4. (a) Proposed tribrachial flame structure and flame image near the bronze porous media, and chemiluminescence images of excited (b) C_2^*, (c) OH*, and (d) CH*.

porous medium causing a back pressure pulse in the liquid fuel line due to rapid vaporization in the previous moment. The flushing process steeply reduces the temperature of the porous cap. In this process, the flame becomes unstable and pulsates back and forth in the chamber. The cycle of dry-out and replenishment of the liquid fuel is the principle cause of flame oscillation and instability. When the air flow rate increases to 355 mg/s, the fluctuation of the bronze is decreased, as shown in Fig. 5c. Increasing swirling air, the flame anchoring will shift downstream and will be less prone to the dry-out-replenishment instability. Interestingly, there is a very-low-frequency fluctuation happening in the stainless steel case in Fig. 5c. It is observed that the hot spot on the porous cap becomes larger and brighter as the air flow rate is increased. The over-heated porous cap will induce minor and very slow dry-out-and-replenishment instability. Flame pulsation is hardly observed, and flame length almost remains constant. Flame pulsation and oscillation are also amplified when added with iron pentacarbonyl for the bronze porous case, as shown in Fig. 5d.

3.3. Flame characteristics of hydrocarbon plus iron pentacarbonyl

Adding iron pentacarbonyl in hydrocarbon fuels is expected to produce high flame luminosity. Figure 6 displays the flame features of the stainless steel porous cap combustor in different iron pentacarbonyl volumetric concentrations at a fixed equivalence ratio of 1.3. It is evident to observe the flame luminosity increasing as the iron pentacarbonyl concentration increases to 0.2 vol.%. Flame color in the post flame region turns to bright sliver-white, and its luminescence intensity is approximately 10.74 mW/mm^2, which is higher than 8.65 mW/mm^2 of the pure *n*-heptane case. Additionally, the flame length is much larger than that of pure *n*-heptane flame due to the reduced flame velocity. Similarly, the luminescence intensity increases to 13.12 mW/mm^2 as the iron pentacarbonyl concentration is increased to 0.6 vol.%. However, red iron oxide can be found to adhere to the top section of the quartz, as shown in Fig. 6c, and reduces transparency of the combustion chamber. The optimization of the iron pentacarbonyl concentration will depend on the tradeoff.

An investigation of stable operation limits is performed over a wide fuel and air flow range, and Fig. 7 shows the limits for different porous materials and fuel compositions. The upper limit defines the flame quenching, while the low limit is determine by dry-out-and-replenishment instability. For the two porous materials, stainless steel has a much wider operation range than bronze, and stable operation can extend to ultra lean condition. Interestingly, there is only low limit in the bronze case when burning pure *n*-heptane. However, after adding 0.2 vol.% iron pentacarbonyl in *n*-heptane, the stable operating ranges for two porous materials become similar, and the low limit for bronze case disappears. As argued above, reducing flame velocity due to iron pentacarbonyl tends to be free from the dry-out-and-replenishment instability. Figure 8 shows the variation of CO and NO_x emissions with the equivalence ratio in different fuel compositions using stainless steel

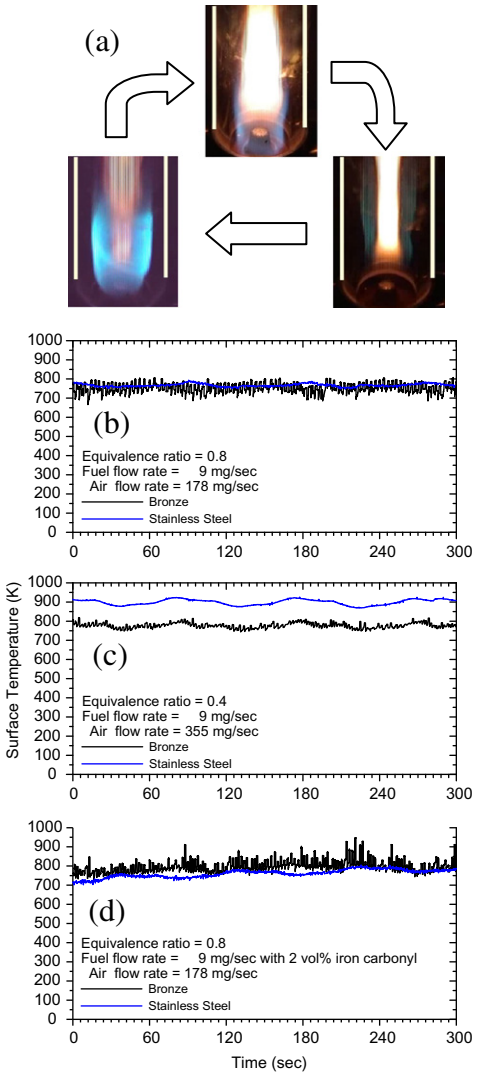

Fig. 5. (a) Combustion oscillation in stable condition, and temperature on the two porous caps in pure *n*-heptane fuel of (b) $\Phi = 0.8$ and (c) $\Phi = 0.4$, and iron pentacarbonyl-doped fuel of (d) $\Phi = 0.8$.

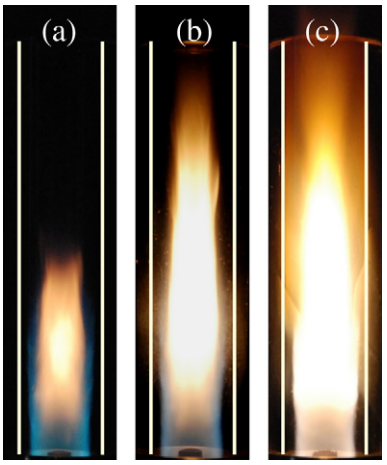

Fig. 6. Flame luminosity in (a) pure *n*-heptane, (b) *n*-heptane with 0.2 vol.% , and (c) *n*-heptane with 0.6 vol.% iron pentacarbonyl in fixed equivalence ratio of 1.05 (exposure time: 1/10 s).

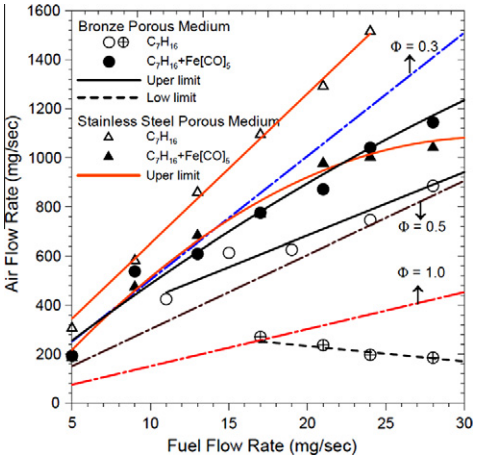

Fig. 7. Stable operational envelopes for different porous medium material and fuel compositions condition.

porous medium. Results indicate that CO emission for the 0.2 vol.% iron pentacarbonyl case is increased slightly, especially in fuel-rich condition. For stainless steel, flame instability happens in the fuel-lean condition, so that its corresponding CO emission is relatively higher than that in fuel-rich condition. As to NO_x emission, all values are below than 10 ppm referred to 12% oxygen due to swirling effect.

3.4. Thermophotovoltaic system demonstration

In order to further utilize the thermal energy in addition to the flame luminosity, an emitter tube is implemented in the central-porous fuel-film combustor. The integrated flame luminosity with emitter illumination in the miniature combustor is shown to improve the radiant efficiency and electrical output. Figure 9 shows the photographs of the combustion chamber operating with an emitter tube in different fuel compositions at fixed equivalence ratio of 1.2. The distance between the porous cap and the emitter tube is approximately 15 mm. It appears that bright flame luminosity congregates in the space between the porous cap and the emitter tube. Faint-blue flame sheet burns along the emitter, and the bottom portion of emitter tube is heated to candescence. Compared Fig. 9a with b, it is found that the flame with iron pentacarbonyl effectively yields intensive sliver-

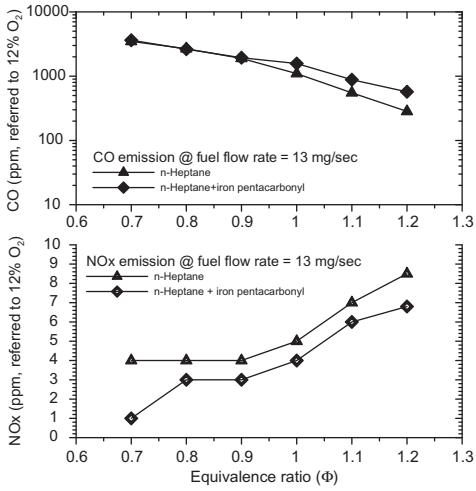

Fig. 8. Effects of equivalence ratio and different fuel composition on (a) CO and (b) NO_x emission using stainless steel porous medium.

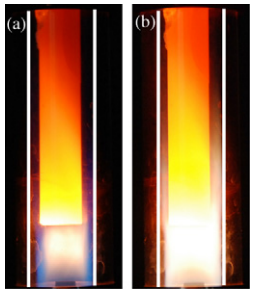

Fig. 9. Combustion chamber operating with an emitter tube for (a) pure *n*-heptane, (b) *n*-heptane plus 0.2 vol.% pentacarbonyl at 15 mg/s and equivalence ration of 1.2 (exposure time: 1/25 s.).

white luminescence, and its flame sheet becomes much longer and brighter along the emitter. It turns out that surface temperature of the emitter becomes more intensive and uniform when burning *n*-heptane with iron pentacarbonyls. The luminescence intensity of the present combustor in the two conditions is measured by using a powermeter. The intensity from the combustor with iron pentacarbonyl flame in Fig. 9b is approximately 125 mW/mm^2, which is much higher than that with pure *n*-heptane flame (22 mW/mm^2). Consequently, high-luminescence flame with an emitter tube can improve the TPV radiant efficiency by more than five folds.

Utilizing a spectrometer to measure the spectrum of the present combustor is performed and the results shown in Fig. 10. We use a plano-concave lens to collect the radiation from the combustor, and the exposure time of the spectrometer is 10 ms. The results indicate that the spectrum of

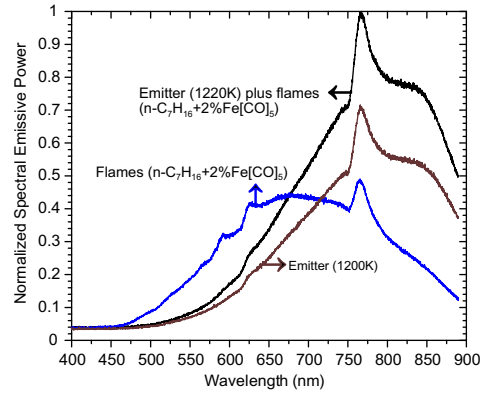

Fig. 10. Spectrum distribution of flame luminosity, emitter radiation, and flame luminosity coupling with emitter radiation.

the flame with iron pentacarbonyl ranges in 550–850 nm and the corresponding high intensity distributes within visible range, while the spectrum of the emitter radiation ranges in 650–900 nm and its corresponding high intensity congregates in the near-infrared. Nevertheless, the spectral distribution of the radiation from the proposed combustor is similar to that from the emitter, but the radiation intensity is more intensive. It is evident that the flame luminosity contributes to an intensity increase in the visible range, and the higher temperature emitter enhances the infrared range of the radiation intensity.

4. Conclusions

A novel conceptual design of a high-luminescent-flame miniature central-porous combustor emitter tube is proposed and tested for application in the TPV power system by adding trace amount of iron pentacarbonyl in *n*-heptane fuel. The main features of the novel combustor design are the central metal-porous fuel injection, and the high-luminescence from the iron pentacarbonyl flame and the emitter tube. Providing a metal-porous medium can result in increasing contact surface and conduction heat transfer for liquid fuel evaporation as well as inhibition of flame quench. Flame structures in different porous medium material are investigated with the use of an intensified camera, and their stabilization mechanisms are speculated as that of the tribrachial flame. The mechanism of flame pulsation and oscillation in the instability range is conjectured to relate to the dry-out-replenishment characteristics. For stable operation, stainless steel porous medium is a proper option for application in TPV power system. The results also show that flame luminosity is significantly enhanced especially in the visible range, and its flame color turns sliver-white. Due

to the low flame emissivity, an emitter tube is implemented in the central-porous fuel-film combustor to enhance the radiant efficiency of the TPV system. Experimental results indicate the radiant intensity of the flame with iron pentacarbonyl in the proposed combustor is more than five times of that of the flame without adding iron pentacarbonyl.

References

[1] M.-H. Wu, Y. Wang, V. Yang, R.A. Yetter, *Proc. Combust. Inst.* 31 (2007) 3235–3242.
[2] D. Dunn-Rankin, E.M. Leal, D.C. Walther, *Prog. Energy Combust. Sci.* 31 (2005) 422–465.
[3] W. Durish, B. Bitnar, F. von Roth, G. Palfinger, *Sol. Energy* 75 (2003) 11–15.
[4] K. Qiu, A.C.S. Hayden, *Energy Convers. Manage.* 47 (2006) 365–376.
[5] K. Qiu, A.C.S. Hayden, *Sol. Energy* 74 (2003) 489–495.
[6] L.G. Ferguson, L.M. Fraas, *Sol. Energy Mater. Sol. Cells* 39 (1995) 11–18.
[7] C. A Wang, H.K. Choi, S.L. Ransom, G.W. Charache, L.R. Danielson, D.M. DePoy, *Appl. Phys. Lett.* 75 (1999) 1305–1307.
[8] L.G. Ferguson, F.A. Dogan, *Mater. Sci. Eng. B* 83 (2001) 35–41.
[9] B. Bitnar, W. Durisch, J.-C. Mayor, H. Sigg, H.R. Tschudi, *Sol. Energy Mater. Sol. Cells* 73 (2002) 221–234.
[10] W.M. Yang, S.K. Chou, C. Shu, H. Xue, Z.W. Li, *J. Phys. D: Appl. Phys.* 37 (2004) 1017–1020.
[11] C.Y. Wu, Y.C. Chao, T.S. Cheng, C.P. Chen, C.T. Ho, *Combust. Flame* 156 (2009) 362–373.
[12] T.C. Williams, C.R. Shaddix, *Combust. Sci. Technol.* 179 (2007) 1225–1230.
[13] D. Reinelt, G.T. Linteris, *Proc. Combust. Inst.* 26 (1996) 1421–1428.
[14] M.D. Rumminger, G.T. Linteris, *Combust. Flame* 128 (2002) 145–164.
[15] W.A. Sirignano, T.K. Pham, D. Dunn-Rankin, *Proc. Combust. Inst.* 29 (2002) 925–931.
[16] W.A. Sirignano, S. Stanchi, R. Imaoka, *J. Prop. Power* 21 (2005) 1075–1091.
[17] Y.H. Li, H.Y. Li, D. Dunn-Rankin, Y.C. Chao, *Prog. Photovolt: Res. Appl.* 17 (2009) 502–512.
[18] Y.H. Li, Y.C. Chao, VDM Verlag Dr. Muller Aktiengesellschaft and Co. KG., 2008.
[19] C.J. Dasch, *Appl. Opt.* 31 (1992) 1146–1152.
[20] T.K. Pham, D. Dunn-Rankin, W.A. Sirignano, *Proc. Combust. Inst.* 31 (2007) 3269–3275.
[21] Y.H. Li, Y.C. Chao, D. Dunn-Rankin, *Combust. Sci. Technol.* 180 (2008) 1900–1919.